Effect of surface hydroxylation on the catalytic activity of a Cr(II)/SiO<inf>2</inf> model system of Phillips catalyst

Effect of surface hydroxylation on the catalytic activity of a Cr(II)/SiO_2 model system of Phillips catalyst

Andriy Budnyk[a, b], Alessandro Damin[a], Elena Groppo[a], Adriano Zecchina[a], Silvia Bordiga[a]

[a] Department of Chemistry, NIS and INSTM Reference Centre, University of Turin, Via G. Quarello 15 A, I-10135 Torino, Italy

[b] Southern Federal University, Zorge Street 5, 344090 Rostov-on-Don, Russia

Abstract

Cr/SiO_2 systems (0.1 wt% of Cr) in the form of high surface area glasses have been synthesized. After proper activation in the 823–1023 K range, they transformed to Cr(VI)/SiO_2 and then to Cr(II)/SiO_2 due to CO reduction (performed at 623 K). Subsequently, C_2H_4 polymerization activity on these samples has been followed. Surprisingly, ethylene polymerization proceeds faster on samples obtained at 823 K, those ones coming from activation at 1023 K resulting less performing. UV–Vis and FT-IR spectroscopies revealed that the progressive increase of activation temperature leads to even more defined and protruding Cr(II) species at highly de-hydroxylated silica surface: this opens new questions on features of active sites and on the role of silica in preparing such species. Finally, the obtained experimental data have been used as references to validate models and methods adopted to simulate the Cr(II)/SiO_2 system, foreseeing to further investigation of the reactivity of Cr(II) toward ethylene.

Graphical abstract

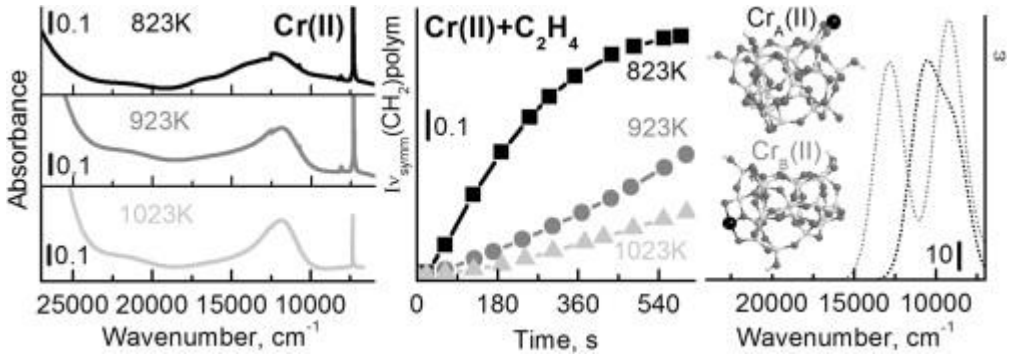

Keywords

- Phillips catalyst;
- Cr-doped porous silica glass;
- Ethylene polymerization;
- UV–Vis spectroscopy;
- FT-IR spectroscopy;
- CO probe molecule;
- Molecular modeling;
- DFT calculations

1. Introduction

The Cr/SiO_2 Phillips catalysts were commercialized for the market of plastics more than a half century ago [1] and still preserve their importance; nowadays, they account for more than 50% of the annual HDPE production and produced different grades of LLDPE as well [2]. Prior to ethylene polymerization, the Phillips-type catalysts have to be "activated" by calcination in dry air (or oxygen) at elevated temperature. During this step, chromium ions in the oxidized state (+6) react with the hydroxyl groups at the silica surface and remain anchored in the form of chromates or, less probably, dichromates and polychromates [3]. Simultaneously, molecular water is released through the condensation of surface hydroxyl groups and the formation of strained siloxane bridges; the dehydroxylation process increases with the rise of temperature. It has been proved that the activation temperature has a strong influence on the catalyst activity toward ethylene polymerization [4]: activity increases with the calcination temperature up to 1173 K and decreases shortly after 1198 K due to the sintering of the silica support. Hence, citing McDaniel, "calcination does something more than just anchor the chromium to the silica surface"; rather, it influences the interplay between the chromium sites and their local environment, which is composed of siloxane rings and terminal hydroxyl groups.

A clear relationship between silica hydroxylation degree, properties of the chromium sites, and catalytic activity is still missing. In the present work, we report a systematic experimental study on the influence of the dehydroxylation state of the silica support on both the catalytic activity of Cr/SiO_2 and the properties of the grafted chromium sites, after activation (outgassing and oxidation in O_2 at elevated temperature to obtain $Cr(VI)/SiO_2$ system) and a successive reduction in CO atmosphere at 623 K ($Cr(II)/SiO_2$). This second step, which affords a stoichiometric reduction of Cr(VI) to Cr(II) sites, is often employed in academic laboratory for characterization purposes, but it is also an industrial practice to pre-reduce the chromium sites before ethylene polymerization, thus shortening the induction period. Notice that Cr(II) sites are simply the precursors of the active species which derive from Cr(II) by oxidative interaction with ethylene. This means that the valence state of Cr in active sites is larger than (II). It is possible that, like found by Coperet et al. [5] and [6] also, Cr(III) can be the precursor of catalytic centers. However, a comparison between the $Cr(II)/SiO_2$ system and the systems described in [5] and [6] must be made with care because of their entirely different structure. The experiments were performed on a Cr-doped glass monolith (obtained by sol–gel method) with chromium loading of 0.1 wt% (i.e., 10 times lower than the usual 1 wt% loading), activated at three different temperatures: 823, 923, and 1023 K. This very low chromium loading, which represents a very innovative aspect of this study, was chosen as the safest method to minimize clustering and hence to enhance the concentration of genuinely isolated Cr(II) sites. Although the method does not fully guarantee that residual nearby Cr(II) sites can still be present, it ensures that their contribution is minimal. Transparent silica xerogels of high surface area, produced through a sol–gel process, were already employed as hosts for transition metal ions [7]. Recently, we demonstrated that mesoporous Cr/SiO_2 monoliths are good models for the industrial Phillips catalysts, with the additional advantage to increase of some order of magnitude the sensitivity of characterization techniques, such as UV–Vis and FT-IR spectroscopies of adsorbed species [8]. Increased sensitivity is mandatory when dealing with such a low concentration of active sites. In this work, Cr(II) sites obtained on CO-reduced parent $Cr(VI)/SiO_2$ systems (obtained in the 823–1023 K interval activation temperatures) have been investigated by means of UV–Vis spectroscopy and FT-IR of adsorbed CO. As catalytic activity is also a sensitive (although indirect) probe of the structure and properties of the catalytic centers, the activity of Cr(II) sites in ethylene polymerization on samples activated at temperatures in the 823–1023 K interval has also been examined.

The experimental results were then used for validating theoretical models of the Cr/SiO_2 catalyst based on a cluster approach. Theoretical calculations provided important details on the geometrical, vibrational and electronic features of anchored chromates, surface Cr(II) species, and Cr(II)···CO adducts, which are useful to correlate the properties of the chromium sites with the observed catalytic activity. Previous studies were based both on periodic (mainly referring to $Cr(VI)/SiO_2$ system) [9] and [10] on hydroxylated surfaces or cluster (devoted to the study of $Cr(II)/SiO_2$ system) [11], [12], [13] and [14] approaches. To the best of our knowledge, this is the first time that the whole set of experimental data obtained on $Cr(II)/SiO_2$ systems characterized by an exceptionally low concentration of chromium sites is compared with computational results. The main issue is thus the definition, by using the experimental data as sole reference, of the accuracy of adopted computational scheme (including the ONIOM embedding approach), which is planned to be employed for further studies of the first stages of ethylene polymerization on reduced model Cr/SiO_2 catalyst.

2. Experimental, computational models and methods

2.1. Experimental

The $Cr(VI)/SiO_2$ samples containing 0.1 wt% of Cr were synthesized in the form of xerogels by the acid-catalyzed sol–gel method; details were already reported elsewhere [8]. This loading is 5–10 times lower than that of industrially employed Phillips catalysts. After gelation and respective thermal treatment, dry xerogel was stabilized at 873 K. The monolith is homogeneously colored in yellow and optically transparent. A pure silica monolith was also synthesized as a reference following the same procedure. For UV–Vis and FT-IR measurements in transmission mode, monolith slices, about 1–2 mm thick, were used (for a final Cr molar content of $1.5 \cdot 10^{-6}$ mol). For surface area measurements, the monoliths were ground into grains before insertion into the measurement apparatus.

The samples were activated in the same cells used for spectroscopic measurements. The activation procedure consisted of a few successive steps: (1) outgassing overnight at room temperature; (2) thermal activation under dynamic vacuum at chosen temperature (823, 923, or 1023 K); during this step, the temperature is gradually raised from room temperature to the desired value, and then, the sample is kept at this temperature for 1 h; (3) oxidation in pure oxygen: oxygen (100 mbar) is dosed twice for 30 min alternated by an outgassing step to remove the reaction products; and (4) cooling to 623 K in the presence of oxygen with subsequent evacuation at the same temperature under dynamic vacuum. The described procedure allows to prepare three $Cr(VI)/SiO_2$ samples activated at 823, 923, and 1023 K. To prepare the corresponding $Cr(II)/SiO_2$ samples, the $Cr(VI)/SiO_2$ systems are further treated in the presence of carbon monoxide at 623 K (two doses of CO of 100 mbar for 30 min alternated by an outgassing step). CO is then removed at 623 K, and the sample is cooled down to room temperature under dynamic vacuum.

FT-IR measurements were performed on a Nicolet 6700 instrument (Thermo Scientific) at a spectral resolution of 2 cm^{-1}. The sample was placed in an IR cell permanently attached to a vacuum manifold allowing gas dosage *in situ*, this setup defining a Cr/ethylene molar ratio of 3:20,000 (when 100 mbar of equilibrium pressure of ethylene are dosed). To quantitatively compare the results obtained on different samples, the FT-IR spectra were normalized to the optical thickness of the samples, by using the IR absorption band at 2242 cm^{-1}, which is characteristic of the silica support.

Optical spectra were collected in transmittance mode on a Varian Cary 5000 spectrophotometer, at spectral resolution of 2 nm. The samples were placed in a quartz cell equipped with optical windows (Suprasil), which allows *in situ* gas dosage.

Textural properties were investigated by N_2 adsorption measurements on a Micromeritics gas analyzer ASAP 2020. The specific surface area (SSA) was evaluated by the BET method [15] and the pore size distribution (PSD) was obtained by applying the BJH method [16] to the desorption branch of the 77 K N_2 isotherms.

2.2. Theoretical methods and models

Calculations were performed by adopting a cluster approach [17] and Gaussian 09 software [18]. To model Cr(II)/SiO_2 systems (in their highly dehydroxylated form), we adopted clusters with the *brutto* formula of $H_6O_{48}Si_{22}Cr$ (see Fig. 1 for their graphical representation, part a and b). The Cr(II) species can be grafted on the silica surface in several positions so originating a plethora of structures which still cannot be all treated with computational methods. In our approach, the Cr(II)/SiO_2 clusters are divided into two models (structures) in terms of the place where the Cr(II) moiety is grafted. In the model represented in Fig. 1a (hereafter model Cr_A(II)), the Cr(II) moiety is saturating two distal Si–O dangling bonds belonging to a five-membered SiO_4 ring. The model represented in Fig. 1b (hereafter model Cr_B(II)) is instead obtained by saturating two distal Si–O dangling bonds inserted in a seven-membered SiO_4 ring.

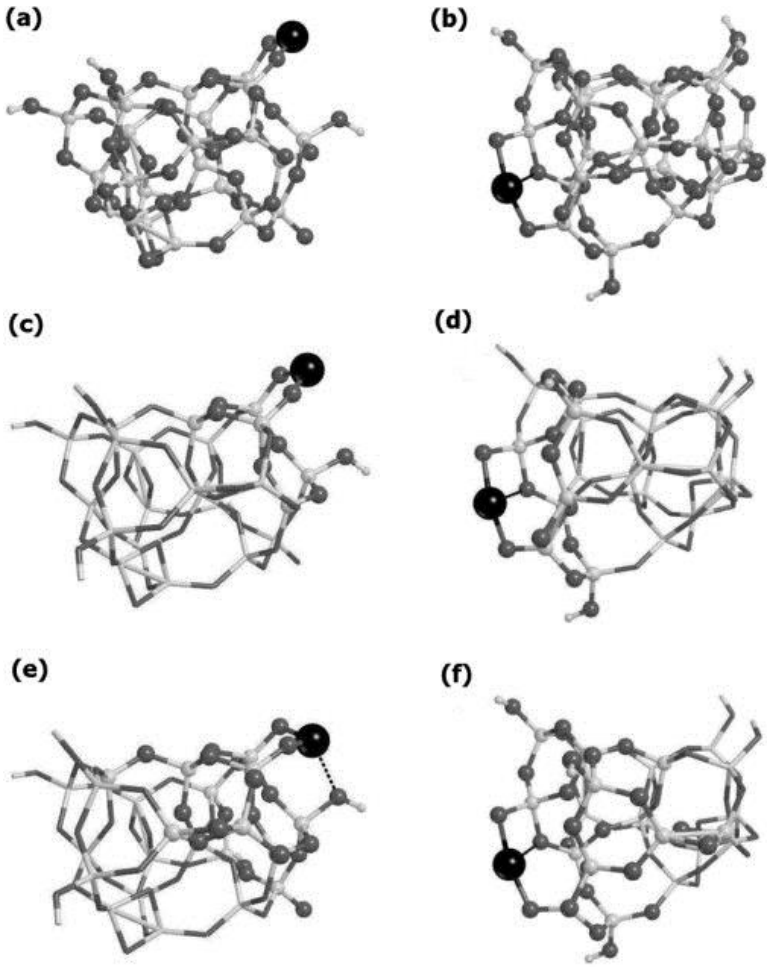

Fig. 1. Graphical representation of Cr_A(II) (a) and Cr_B(II) (b) clusters adopted to model highly dehydroxylated Cr(II)/SiO_2 system. Small white spheres: H atoms. Big white spheres: Si atoms. Gray spheres: O atoms. Black sphere: Cr atom. Structures (c–f) show the graphical representation of both Cr_A(II) and Cr_B(II) models as defined in the ONIOM scheme: (c) Cr_A(II) model for M/R = 0.22, (d) Cr_B(II) for M/R = 0.30, (e) Cr_A(II) for

M/R = 0.48, and (f) Cr_B(II) for M/R = 0.52. M zone is rendered with ball and sticks, while sticks refer to the remaining part of R zone.

In order to reduce the computational cost, the ONIOM embedding approach [19] was employed. A complex system such that employed here is subdivided in n = 2 two layers: the model (M) and the real (R) zones, respectively. The model zone (M) includes a variable portion of the whole system and it is treated at a high (hereafter indicated as H) level of theory, adopting quantum mechanics (hereafter indicated as QM). The real zone (R) is treated at a low (hereafter indicated as L) level of theory: this can be based either on molecular mechanics (hereafter indicated as MM) or on QM-derived methods (but with a poorer basis set). The final energy of a system E(ONIOM) described in the ONIOM scheme, and all the derived quantities (gradients and so on), can be summarized in the following formula:

equation(1): E(ONIOM)=E(HM)+E(LR)-E(LM),E(ONIOM)=E(HM)+E(LR)-E(LM),

where E(HM) and E(LM) are the energies of M portion of the system, determined at H and L level of theory, respectively; E(LR) is the energy of R, calculated at L level of theory.

Structures (c–f) in Fig. 1 show a graphical representation of models Cr_A(II) and Cr_B(II) as defined in the ONIOM scheme: the variable M zone (treated at both H and L level) is underlined by balls and sticks, the remaining part of R (treated at L level only) being represented just by sticks. Mechanical constrains are transferred to M atoms from the remaining part of R, by the so-called "link atoms" (generally H atoms, not showed in Fig. 1 for sake of clarity): these replace the border atoms between M and R and they are included in M. This approach guarantees the neutrality of the M zone. In particular, Fig. 1c and e refer to model Cr_A(II), where M/R = 0.22 and M/R = 0.48, respectively; Fig. 1d and f is instead representing model Cr_B(II), with M/R = 0.30 and M/R = 0.52, respectively.

The Cr_A(II) and Cr_B(II) models were adopted to study the adsorption of CO on Cr(II)/SiO_2. To evaluate the stability of the formed adducts, the binding energy (hereafter labeled as BE, whose positive values indicate stable adducts) has been computed (in the ONIOM scheme and including the CO molecule in the M zone) accordingly to Eqs. (2) and (3).

equation(2)
BE_{nCO}(ONIOM)=BE_{nCO}(HM)+BE_{nCO}(LR)-
BE_{nCO}(LM),BEnCO(ONIOM)=BEnCO(HM)+BEnCO(LR)-BEnCO(LM),

where n = 1, 2 is the number of CO molecules adsorbed at Cr-containing cluster (hereafter labeled with index clust) and each term is defined as:
equation(3)
$BE_{nCO}=E_{clust}+nE_{CO}-E_{clust\ldots nCO}$.BEnCO=Eclust+nECO-Eclust…nCO.

In Eq. (3), BE_{nCO} comprises the energies of the two isolated systems E_{clust} and E_{CO} at their equilibrium geometry without the energy of the formed adduct $E_{clust\ldots nCO}$.

High-level calculations were performed by adopting the ωB97xD long-range corrected hybrid functional [20]; H atoms were described through a standard Pople-type 6-311++G(2d,2p) basis set [21], Cr and Si by an Ahlrichs TZVp (triple zeta valence plus polarization) basis set [22]; and TZV2p Ahlrichs basis set was adopted to describe O atoms (and C when CO adsorption is concerned). Low level is defined by employing the B97D functional [23]; H, Cr, and Si atoms are described with a 6-31G(d,p) basis set [24]; 6-31+G(d,p) basis set [25] was employed for O and C atoms. As dealing with Cr(II), spin multiplicity was set to 2S + 1 = 5 (four unpaired electrons) and

the unrestricted formalism was adopted. The calculations, including full optimizations without symmetry constraints, were performed on $Cr_A(II)$ for M/R = 0.22 (see Fig. 1c) and M/R = 0.48 (see Fig. 1e) and on $Cr_B(II)$ with M/R = 0.30 (see Fig. 1d) and M/R = 0.52 (see Fig. 1f).

Electronic transitions (obtained through the TD-DFT formalism [26]) were computed just for HM. Moreover, as test calculations show that $\Delta\nu_{CO}$ values computed adopting ONIOM frequencies or just HM are only slightly differing, just data coming from HM frequencies, calculations will be presented.

3. Results and discussion

3.1. Kinetics of ethylene polymerization on Cr(II)/SiO_2

The kinetics of ethylene polymerization at 100 mbar of equilibrium pressure at room temperature were studied on three samples of Cr(II)/SiO_2 activated at 823, 923, and 1023 K, respectively, by collecting FT-IR spectra in transmittance mode with 1-min time resolution. The whole set of results obtained within the first 10 min of reaction is shown in Fig. 2 in the $\nu(CH_2)$ stretching region. The spectra were background subtracted and normalized to the thickness of the samples. It is clear that the ethylene polymerization rate is inversely proportional to the activation temperature and that the polyethylene formed is the same in all the cases (as testified by the corresponding IR absorption bands at 2923 cm^{-1}, $\nu_{asymm}(CH_2)$, and at 2853 cm^{-1}, $\nu_{symm}(CH_2)$). A plot of the intensity of the $\nu_{symm}(CH_2)$ absorption band at 2853 cm^{-1} (chosen here as reference band to monitor the polymer growth) versus time (see Fig. 2d) reveals an almost linear dependence within all the investigated time interval for the samples activated at 923 and 1023 K. On the contrary, for the sample activated at 823 K, after a rapid linear growth, the intensity of the band at 2853 cm^{-1} reaches a plateau, which is explained in terms of diffusion problems. The slopes of the linear parts of the three curves give an indication of the relative rate of polymerization [3], which is around the double for the sample activated at 823 K than for those activated at higher temperature. Moreover, although in all the three cases, the reaction starts immediately after admission of ethylene in the reaction cell, a shorter induction period is observed for the sample activated at 823 K. From our previous work [27], which correlates the intensity of the IR absorption bands of growing polyethylene with the decrease in ethylene pressure, it is possible to estimate the polymerization rate. As an example, for the sample activated at 823 K, the resulting polymerization rate is of about 55 s^{-1} mol_{Cr}^{-1} (corresponding to about $5.5 \cdot 10^6$ g_{PE} h^{-1} mol_{Cr}^{-1}). These values are of the same order of magnitude of those reported in the literature for similar systems [28].

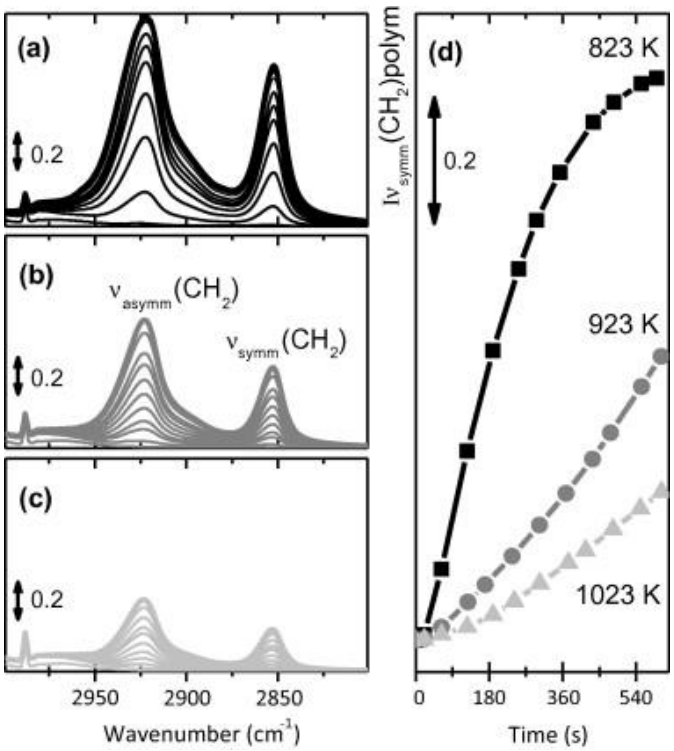

Fig. 2. Kinetics of C_2H_4 polymerization on Cr(II)/SiO_2 catalysts activated at 823, 923, and 1023 K (parts (a), (b), and (c), respectively) as monitored by collecting FT-IR spectra at a time resolution of 1 min. Part (d) shows the intensity of the $\nu_{symm}(CH_2)$ IR absorption band at 2853 cm^{-1} as a function of time, for samples activated at 823 (■), 923 (●), and 1023 K (▲).

These data provide evidence that the lower the activation temperature, the higher the polymerization activity and the shorter the induction period. This result is apparently in contradiction with the general trend reported in the literature [4], where the maximum activity is obtained for catalysts activated at 1198 K. However, it must be noted that the ethylene polymerization kinetics derived from the FT-IR spectra shown in Fig. 2 refer to Cr(II)/SiO_2 catalysts obtained by pre-reduction with CO, whereas the literature data are all related to Cr(VI)/SiO_2 catalysts, where the Cr(VI) is reduced to a low valence state by ethylene. The two processes of reduction are not identical since in the first case, only CO_2 is produced while in the second one, H_2O is generated. Hence, dehydroxylation of the silica support seems to affect the properties of the chromium sites differently according to their oxidation state.

The unexpected results shown in Fig. 2 on the effect of thermal treatments on the polymerization activity form the motivation of a detailed characterization on the effect of activation temperature on the chromium surface species. Due to the model character of the much diluted Cr/SiO_2 systems investigated in this study, the characterization results are compared with computational simulations obtained on suitable models of chromium centers.

3.2. The effect of activation temperature on the hydroxyl population of Cr(II)/SiO_2

The effect of the activation temperature on the obtained Cr(II)/SiO_2 was investigated by means of FT-IR spectroscopy in the 3000–5000 cm^{-1} range (see Fig. 3), where the ν(OH) and ν(OH) + δ(OH) modes involving surface –OH species are expected to contribute at about 3750 and 4500 cm^{-1}, respectively. The background spectra of activated samples are presented in Fig. 3 (normalized to the thickness). Dehydroxylation in the 823–1023 K temperature interval causes a progressive erosion of the IR absorption band at 3750 cm^{-1}, and in particular of its tail at low frequency, which is due to ν(OH) vibrations of –OH groups interacting via weak hydrogen bonds with adjacent groups. This observation can be interpreted in terms of two processes occurring simultaneously, which can be schematically represented as follows:

equation(4)
$$2\equiv\mathrm{Si{-}OH} \rightarrow \mathrm{Si{-}O{-}Si} + \mathrm{H_2O},$$

equation(5)
$$\equiv\mathrm{Si{-}OH}\cdots\mathrm{X} \rightarrow \mathrm{Si{-}OH} + \mathrm{X} \quad (\mathrm{X} = \mathrm{Si{-}O{-}Si}, (\mathrm{SiO})_2\mathrm{CrO}_2).$$

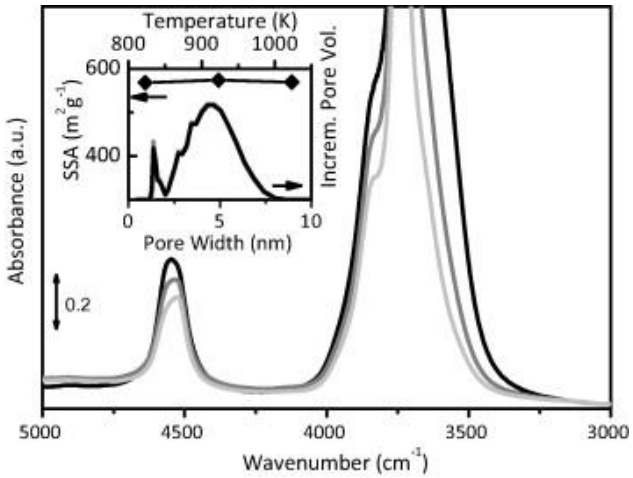

Fig. 3. FT-IR spectra, in the 3000–5000 cm^{-1} range (where the ν(OH) and ν(OH) + δ(OH) modes involving surface –OH species are expected to contribute), of Cr(II)/SiO_2 samples after activation at 823 (black), 923 (dark gray), and 1023 K (light gray). The inset shows the BET-specific surface area values (♦) and the pore size distribution profiles as obtained from BJH analysis.

The first process is the elimination of a water molecule through the condensation of residual surface hydroxyl groups interacting via weak hydrogen bonds. This process is clearly observed here just because the high thickness of the monolith slice allows the observation of hydrogen-bonded –OH groups present also in very small concentration; on the contrary, it is hardly observable on Cr(II)/SiO_2 in the form of thin pellets (less than 0.1 mm thick) utilized so far [3]. Condensation of surface –OH groups is likely associated with a surface reorganization, a fact that might be at the origin of the second simultaneous process (see Eq. (5)). Surface reorganization induced by forced dehydroxylation is expected to play an important role on particles of nanometric dimensions, where the dehydroxylation process does necessarily involve a response of the whole structure. The shoulder at 3840 cm^{-1} is tentatively assigned to a combination mode between the ν(OH) stretching mode and a low frequency SiO_2 skeletal mode of appropriate symmetry.

The IR absorption band at about 4550 cm^{-1} is assigned to the combination of different vibrational modes, involving the Si–OH stretching and the Si–O–H bending modes [29], although its precise assignment is still under debate [30]. In this respect, it is useful to recall that, opposite to the behavior of ν(OH) absorption bands, the δ(OH) bands undergo a shift to higher wavenumber values upon hydrogen-bonding interaction. The sequence of spectra presented in Fig. 3 strongly supports the hypothesis that the 4550 cm^{-1} band involves preferentially δ(OH) vibrational modes. In fact, dehydroxylation at increasing temperature causes the preferential erosion of the high frequency part of the absorption band. Nevertheless, the assignment of this absorption band in terms of sole combination of ν(OH) + δ(OH) modes is not fully convincing. In fact, it does not explain why this band still shows a high frequency shoulder even after degassing at 1073 K, which is a situation where hydrogen bonding is minimized. For this reason, the participation of a skeletal mode (as observed for the high frequency shoulder of the ν(OH) mode) must be invoked.

The given assignments are based on the implicit assumption that the texture of the sample does not appreciably change upon activation at progressively increasing temperature up to 1073 K. In order to exclude that applied thermal treatment may cause significant changes in the textural properties of the silica support, nitrogen adsorption/desorption measurements were performed on pure silica samples activated in the same way as Cr/SiO_2 samples. The physisorption isotherms (here not shown for sake of brevity) are very similar irrespective of the activation temperature, all being of type IV (IUPAC) [31], which is typical for mesoporous materials. For all samples, the calculated BET SSA values are about 570 $m^2\ g^{-1}$, and the PSD is centered on 4.5 nm (see inset in Fig. 3). To understand the reasons of the stability of the monolith toward thermal treatments, it is useful to recall that its stabilization temperature of 873 K was reached very slowly, thus allowing reconfiguration of the network and relaxation of siloxane rings. Hence, dehydroxylation occurs without appreciable reduction of the surface area or pore dimension. In turn, this implies that any difference in the catalytic activity of Cr/SiO_2 samples activated in the 823–1073 K interval should originate from a difference in the structure of the Cr sites, which in turn might be influenced by neighboring hydroxyls distribution and surface reconstruction associated with high dehydroxylation.

3.3. Properties of Cr(II)/SiO_2 as monitored by UV–Vis spectroscopy and FT-IR spectroscopy of adsorbed CO

3.3.1. Experimental results

The Cr(II)/SiO_2 samples obtained upon reduction in CO of the corresponding Cr(VI)/SiO_2 samples were characterized by UV–Vis spectroscopy in transmittance mode. The UV–Vis spectra are shown in Fig. 4a–c in the 25,000–5000 cm^{-1} region, where d–d electronic transitions are visible; at higher wavenumbers, the spectra are dominated by the very intense and out of scale absorptions due to

charge-transfer transitions. The UV–Vis spectra of the three Cr(II)/SiO_2 samples are similar, although the absorption bands are more intense and narrower upon increasing the activation temperature. In particular, in all the spectra a couple of absorption bands are observed, at about 12,000 and 7200 cm^{-1}; these bands were previously observed in the UV–Vis spectra of Cr/SiO_2 samples in the powder form, and attributed to d–d electronic transitions of coordinatively unsaturated Cr^{2+} species [32]. Two additional weak bands are observed at about 21,400 and 17,000 cm^{-1}, whose assignment is not yet clear. Hence, UV–Vis spectroscopy provides an evidence that the Cr(II) sites in our Cr(II)/SiO_2 monoliths have electronic properties very similar to those of the parents Cr(II)/SiO_2-powdered samples.

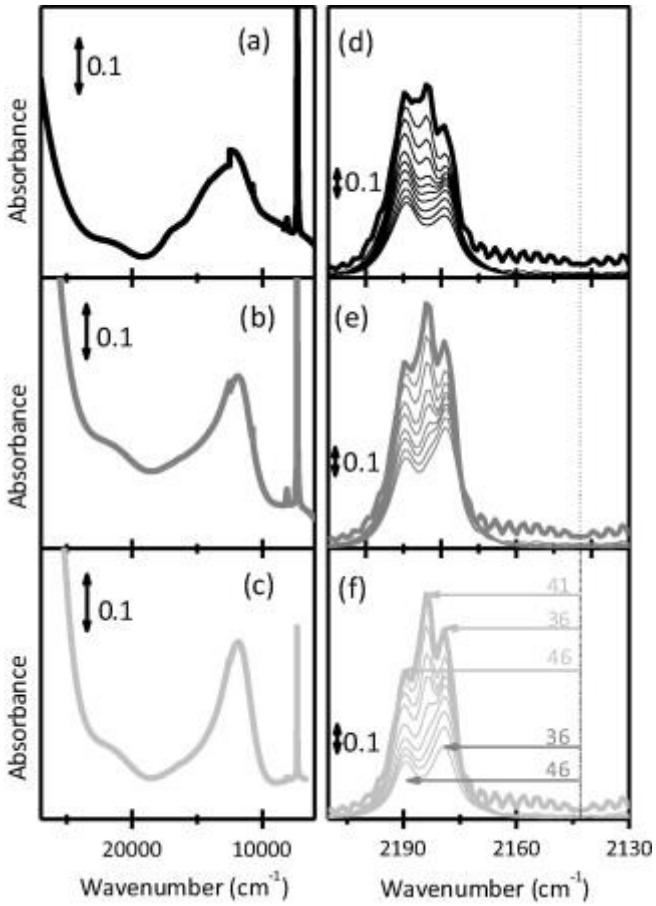

Fig. 4. Parts (a–c): UV–Vis spectra of 0.1 wt% Cr(II)/SiO_2 obtained upon reduction in CO of the corresponding Cr(VI)/SiO_2 samples activated at 823 (a), 923 (b), and 1023 K (c). Parts (d–f): FT-IR spectra of CO adsorbed at room temperature on the same Cr(II)/SiO_2 samples of parts (a–c). The three sequences of spectra are collected upon decreasing the CO coverage; bold spectrum corresponds to the maximum CO coverage. Dotted line indicates the ν(CO) of CO in the gas phase; the arrows in part (f) show the shift of the ν(CO) absorption bands with respect to the gas phase.

The same Cr(II)/SiO_2 samples were successively investigated by means of FT-IR spectroscopy of CO adsorbed at room temperature. This method was demonstrated in the past [3] to efficiently distinguish among Cr(II) sites characterized by a different degree of coordinative unsaturation: Cr_A(II) sites are able to coordinate up to two CO molecules at room temperature, whereas Cr_B(II) sites form only mono-carbonyl adducts. Fig. 4d–f shows the FT-IR spectra of CO adsorbed at room temperature (bold curves) on the three Cr(II)/SiO_2 samples of Fig. 4a–c, and the evolution of the spectra upon decreasing the CO coverage. In all the three cases, the FT-IR spectra collected at the maximum CO coverage show three distinct absorption bands at 2190, 2184, and 2179 cm^{-1}, which were observed also on Cr/SiO_2 catalysts [33] and were assigned to the formation of di-carbonyl and mono-carbonyl adducts on Cr_A(II) and Cr_B(II) sites, respectively. Upon decreasing the CO coverage, the doublet at 2184 and 2179 cm^{-1} reduces to a single band at 2179 cm^{-1}, corresponding

to transformation of di-carbonyl to mono-carbonyl adducts on $Cr_A(II)$ sites, as already well documented for Cr/SiO_2 catalysts. The relative intensity of the IR absorption bands at 2190, 2184, and 2179 cm^{-1} significantly changes in the three series of spectra. In particular, the band at 2190 cm^{-1} is much more pronounced after activation at 823 K (Fig. 4d), whereas the couple of bands at 2184 and 2179 cm^{-1} progressively increases in intensity with increasing the activation temperature. This observation suggests that the relative population of $Cr_A(II)$ and $Cr_B(II)$ sites is considerably affected by the activation procedure, as previously demonstrated for Cr/SiO_2 catalysts.

3.3.2. Theoretical calculations

The UV–Vis and FT-IR data collected on the $Cr(II)/SiO_2$ system (see Fig. 4) were successively compared with the results of a theoretical analysis performed on the reduced chromium models shown in Fig. 1. The principal geometrical features of the optimized $Cr_A(II)$ and $Cr_B(II)$ models are resumed in Table 1. The surrounding of $Cr_A(II)$ is affected by the choice of the M/R zone ratio: in fact, for M/R = 0.22, the modeled $Cr_A(II)$ site is isolated, whereas for M/R = 0.48, it interacts with both nearby silanol moiety and a siloxane bridge belonging to the silica framework (see Table 2, Cr···O distances). This causes an elongation of the average 〈Cr–O〉 bond, which moves from 〈1.837〉 Å to 〈1.889〉 Å. Whatever is the M/R ratio, the optimized $Cr_A(II)$ site is quite protruding from the first neighboring oxygen atoms. The HOMO(LUMO), partially filled by one of the four unpaired electrons of high spin Cr(II), is centered on Cr atom and has a "d_{xy}"("d_{x2-y2}") character. On the contrary, in $Cr_B(II)$ model (〈Cr–O〉 = 1.939 Å), the Cr(II) site is quite buried and also strongly interacting with a third oxygen atom coming from a siloxane bridge (see Table 2 for the geometrical features. The HOMO(LUMO) orbital is again centered on Cr atom and it has a "d_{x2-y2}"("d_{xz}") character. It is interesting to notice that by reversing the occupancy of HOMO–LUMO orbitals in $Cr_B(II)$ model, it is possible to get a protruding Cr(II) species, but in this case, the overall structure resulted to be less stable than before of about 24 kJ mol^{-1} (M/R = 0.52). For $Cr_A(II)$ model instead, no other than Cr(II) protruding species can be obtained, even starting from geometry and HOMO–LUMO ordering typical for a buried species. A possible explanation for this behavior could be found by considering that $(SiO)_2Cr(II)$ species belong to rings with 5 and 7 membering for $Cr_A(II)$ and $Cr_B(II)$, respectively, which allow Cr(II) to reach different equilibrium structures.

Table 1. Calculated bond lengths (Å) and angles (degrees) for the $Cr_A(II)$ and $Cr_B(II)$.

Model	M/R	Cr–O	O–Cr–O	Cr···O
$Cr_A(II)$	0.22	1.841–1.833	120.2	3.929–3.208
$Cr_A(II)$	0.48	1.892–1.885	111.9	2.674–2.475
$Cr_B(II)$	0.30	1.946–1.926	161.1	3.164–2.051
$Cr_B(II)$	0.52	1.949–1.928	161.1	3.138–2.054

Note: Cr···O distances refer to second next O neighbors of Cr.

Table 2. Calculated bond lengths (Å) and angles (degrees) for mono-carbonyl adducts formed at the $Cr_A(II)$ and $Cr_B(II)$ sites.

Model	M/R	Cr–O	O–Cr–O	Cr···O	Cr···CO	$\Delta_{C\equiv O}$
$Cr_A(II)$	0.22	1.886–1.864	112.1	3.317–2.943	2.141	−0.006
$Cr_A(II)$	0.48	1.888–1.868	111.2	3.324–2.913	2.139	−0.005
$Cr_B(II)$	0.30	1.945–1.936	160.7	3.268–2.105	2.126	−0.006
$Cr_B(II)$	0.52	1.950–1.938	160.4	3.253–2.106	2.123	−0.005

Note: Cr···O distances refer to second next O neighbors of Cr.

The computed electronic transitions on Cr_A(II) (M/R = 0.48) and Cr_B(II) (M/R = 0.52) were employed to generate the UV–Vis spectra reported in Fig. 5 (black and gray dotted lines are representative for Cr_A(II) and Cr_B(II) models, respectively). As experimentally observed, the computed spectra are characterized by weak signals in the 7000–13,000 cm^{-1} (which have been assigned to "d–d" transitions), and strong absorption from 25,000 up to 45,000 cm^{-1} (not fully shown in Fig. 4e), which can be assigned to electronic transitions having a charge-transfer character. The UV–Vis spectra obtained on the two models significantly differ in the "d–d" transition region (7000–13,000 cm^{-1}) and even more in the charge-transfer one (25,000–45,000 cm^{-1}). The UV–Vis spectrum simulated for the Cr_A(II) model shows two quite close bands in the "d–d" region, which are responsible of a broad absorption in the 9000–10,500 cm^{-1} interval. On the contrary, the UV–Vis spectrum of Cr_B(II) model is characterized by two quite well-resolved bands located, respectively, at about 9000 and 12,000 cm^{-1}. It is worthy of note that the most intense band in the experimental spectra shown in Fig. 4a–c is well reproduced by superimposing the bands at 10,500 and 12,000 cm^{-1}. The absorption band at 7000 cm^{-1}, well visible in the experimental spectra (although of low intensity), is absent in the computed spectra, suggesting that in both models, the Cr surroundings are not perfectly described.

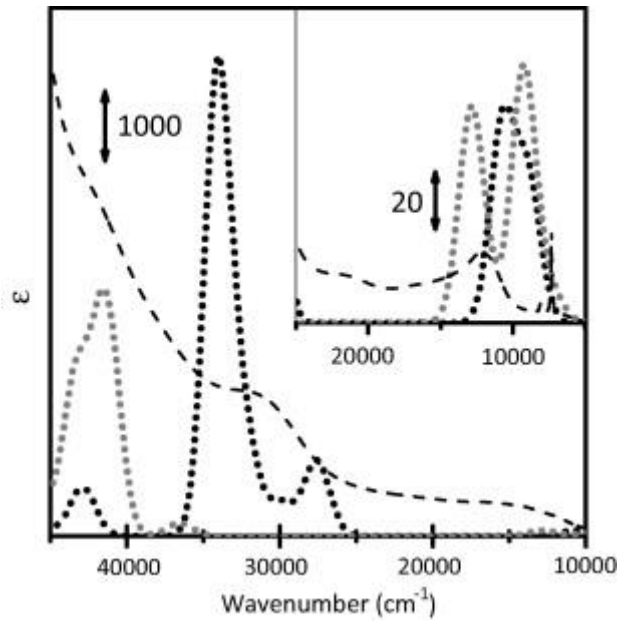

Fig. 5. Computed UV–Vis spectra for Cr_A(II) (black dotted) and Cr_B(II) (gray dotted) models. The inset shows a magnification of the d–d transition region. Experimental spectra are shown by dashed lines.

As far as the charge-transfer region is concerned, it is evident that region is strongly affected by the Cr arrangements. In the simulated UV–Vis spectrum of Cr_A(II), the first charge-transfer transition appears around 27,500 cm^{-1}, followed by a very intense band at about 34,000 cm^{-1} (i.e., 4000 cm^{-1} above the experimental one). On the contrary, the main transition in the UV–Vis spectrum of Cr_B(II) appears at about 41,500 cm^{-1}. From the above discussed data, it can be reasonably concluded that the experimental UV–Vis spectrum is the result of a superimposition of contributions coming from Cr(II) species characterized by two main arrangements, as those obtained for Cr_A(II) and Cr_B(II) models.

Both Cr_A(II) and Cr_B(II) models form quite stable Cr(II)···CO adducts, as testified by the positive values of BE reported in Fig. 7a and b (gray and black lines for mono- and di-carbonyls, respectively). The geometrical details of mono-carbonyl and di-carbonyl adducts on both Cr_A(II) and Cr_B(II) are summarized in Table 2 and Table 3, respectively, whereas their graphical

representations are shown in Fig. 6a–d. For mono-carbonyls, the computed ONIOM BEs are in the 70–80 kJ mol^{-1} range (and are only slightly affected by the M/R ratio), Cr_B(II) mono-carbonyl being slightly more stable with respect to the Cr_A(II) one (85.3 versus 72.3 kJ mol^{-1} when M/R = 0.52 and M/R = 0.48 are considered, respectively). It is worth noticing here that such values are in good agreement with the observation (coming from IR spectroscopy, see Fig. 4 and previous discussion) that mono-carbonyls formed at Cr(II)/SiO_2 are stable at room temperature. Cr_A(II) and Cr_B(II) possess a different ability to coordinate a second CO molecule: for Cr_A(II), the BE ONIOM (M/R = 0.48) for di-carbonyls formation is 137.7 kJ mol^{-1} (i.e., about the double than that for mono-carbonyls), whereas for Cr_B(II), it is only 116.9 kJ mol^{-1} (M/R = 0.52), and with a net gain with respect to the corresponding mono-carbonyl, of just 31.5 kJ mol^{-1}. The calculated energies are in well agreement with the experimental data previously discussed and coming from FT-IR spectroscopy.

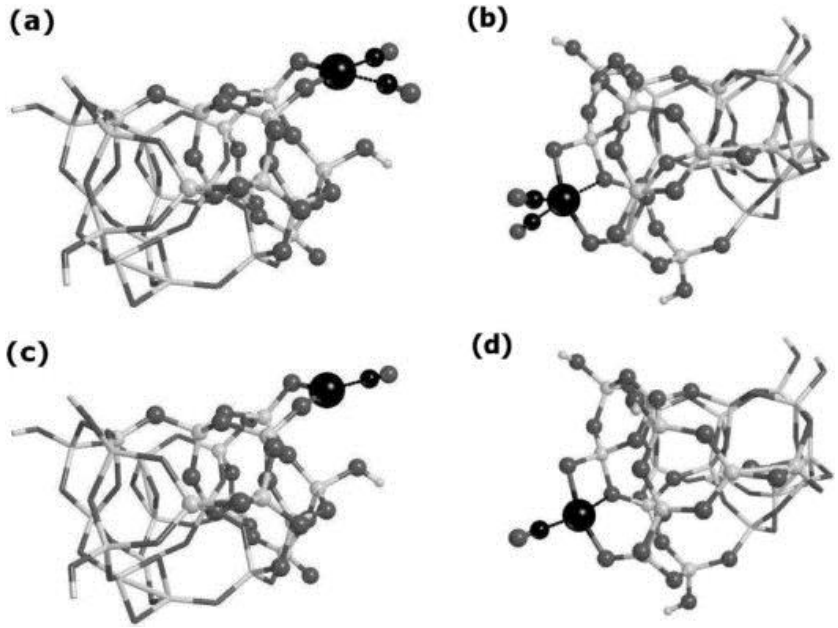

Fig. 6. Graphical representation of optimized di- and mono-carbonyl adducts on Cr_A(II) and Cr_B(II), as defined in the ONIOM scheme: (a) di-carbonyl on Cr_A(II), M/R = 0.48; (b) di-carbonyl on Cr_B(II), M/R = 0.52; (c) mono-carbonyl on Cr_A(II), M/R = 0.48; and (d) mono-carbonyl on Cr_B(II), M/R = 0.52. The graphical details are the same as in Fig. 1, and small black spheres represent C atoms.

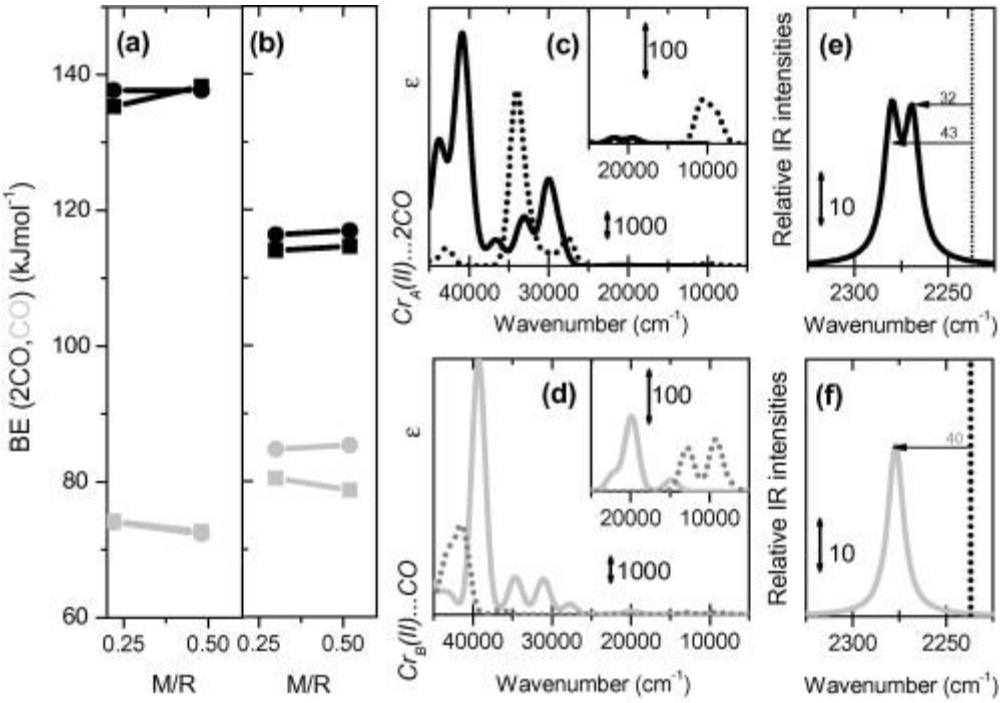

Fig. 7. Part (a): ONIOM BEs (circles) computed for the interaction of one CO molecule (gray) and two CO molecules (black) with Cr_A(II) and Cr_B(II) sites, respectively. HM BEs (squares) are reported for the sake of comparison. Calculated electronic (c and d) and vibrational (e and f) spectra for Cr_A(II) (c and e) and Cr_B(II) (d and f) models in interaction with carbon monoxide. The insets in panels (c and d) are magnifications of the d–d spectral regions. Curves by dotted line represent respective Cr(II) model before interaction with CO molecule.

Table 3. Calculated bond lengths (Å) and angles (degrees) for di-carbonyl adducts formed at the Cr_A(II) and Cr_B(II) sites.

Model	M/R	Cr–O	O–Cr–O	Cr···O	Cr···CO	$\Delta_{C\equiv O}$
Cr_A(II)	0.22	1.916–1.906	101.9	3.152–2.973	2.177–2.161	−0.006/−0.006
Cr_A(II)	0.48	1.919–1.909	101.6	3.164–2.949	2.174–2.161	−0.005/−0.005
Cr_B(II)	0.30	1.958–1.943	158.9	3.688–2.211	2.311–2.147	−0.005/−0.005
Cr_B(II)	0.52	1.959–1.943	158.3	3.698–2.206	2.307–2.147	−0.004/−0.005

Note: Cr···O distances refer to second next O neighbors of Cr.

The computed UV–Vis spectra for the carbonyl adducts shown in Fig. 6 are reported in Fig. 7 (parts (c) and (d), full gray and black lines). It is evident that CO adsorption strongly perturbs the electronic features of both Cr_A(II) and Cr_B(II) clusters, both in the "d–d" and in the charge-transfer regions. In particular, a blueshift of the "d–d" transitions is observed for both models, in good agreement with the experimental data present in the literature [3]. It is worth noticing that only the Cr_B(II) model is able to reproduce the band at about 20,000 cm^{-1} (well visible in the experimental spectra), already for CO mono-carbonyl formation. In the charge-transfer region, the computed spectra of mono- and di-carbonyls on Cr_A(II) and Cr_B(II) models show an opposite behavior: the absorption bands of carbonyl adducts on Cr_A(II) are blueshifted with respect to those of bare Cr_A(II), whereas those of carbonyls formed on Cr_B(II) models last are substantially redshifted (in particular when mono-carbonyl adduct is concerned, see full gray line in Fig. 7d). It is however clear that, by superimposing all the computed spectra, a complex envelope is obtained that, in the charge-transfer region, is substantially blueshifted with respect to the first transitions computed for bare Cr_A(II) model: this reproduces quite well the observed modifications of the experimental UV–Vis spectra, obtained on Cr(II)/SiO_2 system interacting with CO probe molecule. For clarity of Fig. 7, the peaks of mono-carbonyls are omitted.

As previously discussed, CO interaction with Cr(II) species at Cr(II)/SiO_2 surface can be easily followed by IR spectroscopy too (see Fig. 4d–f): for this reason, Cr_A(II) and Cr_B(II) CO adducts have been used to compute the IR spectra reported in Fig. 7 (parts (e) and (f), respectively), to verify if the here employed models (and the adopted computational scheme) are able to reproduce one of the most significative experimental datum (Δν*CO*), which can give indications about Cr(II) environment and its chemical properties, as charge-transfer processes and electrostatics involved in defining the Cr(II)···CO interaction contribute to perturb CO vibrational properties.

In close contact with experiments (see Fig. 4f and e–f), both Cr_A(II) and Cr_B(II) carbonyl adducts are characterized by positive Δν*CO* (in the range quite near to the experimental values). Computed Δν*CO* for mono-carbonyls on Cr_A(II) and Cr_B(II) differs from each other by 8 cm^{-1}, Cr_B(II) giving higher value of Δν*CO* when compared with Cr_A(II), reproducing quite well the situation observed for Cr(II)/SiO_2 at low CO coverage. From this, it can be inferred that the observed CO low-coverage peaks, assigned to Cr_A and Cr_B sites, are reconducible to Cr sites characterized by features reproduced in Cr_A(II) and Cr_B(II) models, respectively. This is further confirmed by two main facts: (i) Cr_B(II) model gives di-carbonyls of very low stability (see Fig. 7b, black curves), so difficult to be observed at RT and reproducing quite well the behavior of the Cr_B carbonyl peak which does not evolve, with pressure, to a doublet characteristic for di-carbonyls species; (ii) Cr_A(II) model gives very stable di-carbonyls (see Fig. 7a, black curves) and Δν*CO* quite close to those one of pressure dependent doublet well observable in the experimental spectrum (see Fig. 4e and black curve of Fig. 7e).

4. Conclusions

Mesoporous high surface area glass monolith doped with 0.1 wt% of chromium (a figure 10–20 times lower than the chromium loading characteristic of the Phillips catalysts) is an ideal system for fundamental studies on the structure and activity of chromium catalytic centers, for at least three main reasons: (i) the chromium sites are genuinely isolated and with mononuclear character; (ii) the silica surface area does not decline with activation temperature in the 823–1023 K range; and (iii) due to the absence of scattering, glass monoliths are properly designed for the determination of many physical properties.

The core of the paper is the unexpected experimental observation that the activity in ethylene polymerization of the reduced catalyst Cr(II)/SiO_2 increases upon decreasing the activation temperature. This result is apparently in contradiction with the opposite trend reported in the literature for industrial catalysts, where ethylene is contacted directly with the oxidized sample, Cr(VI)/SiO_2.

These facts brought us to systematically investigate the hydroxylation state of the surface on the Cr(II)/SiO_2 sample as a function of the activation temperature in the 823–1023 K interval, in terms of distribution of fully isolated and weakly interacting (via hydrogen bonds) hydroxyl groups. The FT-IR spectra of monoliths slices, being characterized by high thickness and total absence of scattering, proved to be ideal for revealing the presence of hydroxyl groups weakly interacting with adjacent species. We observe a systematic reduction of hydroxyl population at the surface, due to the increase of activation temperature, this fact being accompanied by the appearance of more homogeneous Cr(II) sites, as proved by UV–Vis-NIR spectra collected in transmission mode and by FT-IR spectra of Cr(II)–$(CO)_n$ adducts. These observations prove that a higher activation temperature induces a stable rearrangement of the siliceous framework surrounding the Cr(II) centers, which is reflected into a change of the frequency of adsorbed CO.

At this stage of the investigation, being aware that we were in possess of a wide number of experimentally observed physical properties on anchored Cr(II) species, and on samples characterized by a variable silanols population (both isolated and hydrogen bonded to adjacent groups), we became stimulated to apply theoretical models of the Cr/SiO_2 catalyst based on a cluster approach (including the ONIOM embedding approach) based on a single functional. The main scopes were helping the assignment of the experimental data (coming from both electronic and vibrational spectroscopies) and the definition, by using the whole set of experimental data as sole reference, of the accuracy of adopted computational scheme (in terms of adopted models and the employed DFT-based functional). To our knowledge, this is the first time that the whole set of experimental data obtained on $Cr(II)/SiO_2$ systems characterized by exceptional low concentration of Cr sites is compared with computational results based on a single functional. A nonsecondary aim of this philosophy was the validation of a theoretical method which is planned to be employed for further studies of the first stages of ethylene polymerization on reduced model catalyst. Two basic cluster structures were adopted. In the first one, Cr(II) species is saturating two distal Si–O dangling bonds belonging to a five-membered SiO_4 ring. These sites (Cr_A) are highly coordinatively unsaturated and readily lead to $Cr(II)–(CO)_2$ species upon CO dosage. In the second structure (Cr_B), the Cr(II) species are anchored on seven-membered rings and easily form mono-carbonylic species. The two adopted cluster models satisfactorily reproduce the main experimental data: in fact, good agreement is obtained for the d–d and charge-transfer bands of Cr(II) species both before and after CO adsorption and finally for the vibrational properties of $Cr(II)–(CO)_n$ species. The comparison between experimental and theoretical data demonstrates that Cr_A and Cr_B sites coexist on the real surface and that their relative ratio can be altered by the activation temperature.

Acknowledgment

The work has been financially supported by FIRB (RBAP115AYN).

References

[1] J.P. Hogan, R.L. Banks, Polymers and Production Thereof, #2,825,721, U.S.P. Office, United States, 1958.
[2] T.J. Pullukat, R.E. Patterson, Porous silica in transition metal polymerization catalysts, in: R. Hoff, R.T. Mathers (Eds.), Handbook of Transition Metal Polymerization Catalysts: Technology & Engineering, John Wiley & Sons, 2010 (29–52 (see p. 31), 640 p.) (Chapter 2).
[3] E. Groppo, C. Lamberti, S. Bordiga, G. Spoto, A. Zecchina, Chem. Rev. 105 (2005) 115–183.
[4] M.P. McDaniel, Adv. Catal. 53 (2010) 123–606.
[5] M.P. Conley, M.F. Delley, G. Siddiqi, G. Lapadula, S. Norsic, V. Monteil, O.V. Safonova, C. Copéret, Angew. Chem. Int. Ed. 53 (2014) 1872–1876.
[6] M.F. Delley, F. Núñez-Zarur, M.P. Conley, A. Comas-Vives, G. Siddiqi, S. Norsic,V. Monteil, O.V. Safonova, C. Copéret, PNAS 111 (2014) 11624–11629.
[7] A.E. Stiegman, H. Eckert, G. Plett, S.S. Kim, M. Anderson, A. Yavrouian, Chem. Mater. 11 (1993) 1591–1594.
[8] A. Budnyk, A. Damin, C. Barzan, E. Groppo, C. Lamberti, S. Bordiga, A. Zecchina, J. Catal. 308 (2013) 319–327.
[9] H. Guesmi, F. Tielens, J. Phys. Chem. C 116 (2012) 994–1001.
[10] J. Handzlik, R. Grybos, F. Tielens, J. Phys. Chem. C 117 (2013) 8138–8149.
[11] Ø. Espelid, K.J. Børve, J. Catal. 205 (2002) 177–190.
[12] Ø. Espelid, K.J. Børve, J. Catal. 205 (2002) 366–374.
[13] A. Damin, J.G. Vitillo, G. Ricchiardi, S. Bordiga, C. Lamberti, E. Groppo, A. Zecchina, J. Phys. Chem. A 113 (2009) 14261–14269.
[14] L. Zhonga, M.-Y. Lee, Z. Liu, Y.-J. Wanglee, B. Liu, S.L. Scott, J. Catal. 293 (2012) 1–12.
[15] S. Brunauer, P.H. Emmett, E. Teller, J. Am. Chem. Soc. 60 (1938) 309–319.

[16] E.P. Barrett, L.G. Joyner, P.P. Healenda, J. Am. Chem. Soc. 73 (1951) 373–380.
[17] J. Sauer, P. Ugliengo, E. Garrone, V.R. Saunders, Chem. Rev. 94 (1994) 2095– 2160.
[18] M.J. Frisch, G.W. Trucks, H.B. Schlegel, G.E. Scuseria, M.A. Robb, J.R. Cheeseman, G. Scalmani, V. Barone, B. Mennucci, G.A. Petersson, H. Nakatsuji, M. Caricato, X. Li, H.P. Hratchian, A.F. Izmaylov, J. Bloino, G. Zheng, J.L. Sonnenberg, M. Hada, M. Ehara, K. Toyota, R. Fukuda, J. Hasegawa, M. Ishida, T. Nakajima, Y. Honda, O. Kitao, H. Nakai, T. Vreven, J.A. Montgomery Jr., J.E. Peralta, F. Ogliaro, M. Bearpark, J.J. Heyd, E. Brothers, K.N. Kudin, V.N. Staroverov, R. Kobayashi, J. Normand, K. Raghavachari, A. Rendell, J.C. Burant, S.S. Iyengar, J. Tomasi, M. Cossi, N. Rega, J.M. Millam, M. Klene, J.E. Knox, J.B. Cross, V. Bakken, C. Adamo, J. Jaramillo, R. Gomperts, R.E. Stratmann, O. Yazyev, A.J. Austin, R. Cammi, C. Pomelli, J.W. Ochterski, R.L. Martin, K. Morokuma, V.G. Zakrzewski, G.A. Voth, P. Salvador, J.J. Dannenberg, S. Dapprich, A.D. Daniels, Ö. Farkas, J.B. Foresman, J.V. Ortiz, J. Cioslowski, D.J. Fox, Gaussian 09, Revision D.01, Gaussian Inc., Wallingford, CT, 2009.
[19] S. Dapprich, I. Komáromi, K.S. Byun, K. Morokuma, M.J. Frisch, J. Mol. Struct. – THEOCHEM 461-462 (1999) 1–21.
[20] J.-D. Chai, M. Head-Gordon, Phys. Chem. Chem. Phys. 10 (2008) 6615–6620.
[21] P.C. Hariharan, J.A. Pople, Theor. Chim. Acta 28 (1973) 213–222.
[22] A. Schäfer, C. Huber, R. Ahlrichs, J. Chem. Phys. 100 (1994) 5829–5835.
[23] S. Grimme, J. Comp. Chem. 27 (2006) 1787–1799.
[24] R. Ditchfield, W.J. Hehre, J.A. Pople, J. Chem. Phys. 54 (1971) 724–728.
[25] W.J. Hehre, R. Ditchfield, J.A. Pople, J. Chem. Phys. 56 (1972) 2257–2261.
[26] E. Runge, E.K.U. Gross, Phys. Rev. Lett. 52 (1984) 997–1000.
[27] E. Groppo, A. Damin, C. Otero Arean, A. Zecchina, Chem. Eur. J. 17 (2011) 11110–11114.
[28] S.L. Scott, J. Amor Nait Ajjou, Chem. Eng. Sci. 56 (2001) 4155–4168.
[29] A. Burneau, C. Carteret, Phys. Chem. Chem. Phys. 2 (2000) 3217–3226.
[30] A.M. Efimov, V.G. Pogareva, Chem. Geol. 229 (2006) 198–217.
[31] (a) IUPAC Recommendations, Pure Appl. Chem. 57 (1985) 603–619.; (b) IUPAC Recommendations, Pure Appl. Chem. 66 (1994) 1739–1758.
[32] B.M. Weckhuysen, R.A. Schoonheydt, J.M. Jehng, I.E. Wachs, S.J. Cho, R. Ryoo, S. Kijlstra, E. Poels, J. Chem. Soc. Faraday Trans. 91 (1995) 3245–3253.
[33] A. Zecchina, E. Garrone, G. Ghiotti, S. Coluccia, J. Phys. Chem. 79 (1975) 972–978.